Microfluidic flow splitter shape optimization for high throughput

Christoffer Palmér (BME–20), Joel Linder (BME–20)

***Abstract*—Due to an increasing incidence rate, the need for new effective methods for diagnosing cancer are of high importance. Studies have shown that circulating tumor cells, CTCs, have great potential as a diagnostic biomarker. Acoustophoresis is a label free method, capable of separating CTCs from red blood cells in a blood sample. In theory, this would enable better CTC detection than the gold standard method of today, and in turn a better way of diagnosing cancer. However, due to inertial forces, the particles are pushed closer to the centerline of the channel in a phenomenon known as the spillover effect. This occurs without the influence of acoustophoresis, and minimizing the effect is a prerequisite for acoustophoretic separation to work at high throughput. The aim of this project was to verify that the spillover effect could be decreased by changing the shape of the fluid splitter, as has been suggested by previous studies. This was done using genetic algorithms—algorithms that utilize the concept of biological evolution in order to reach optimal solutions. The results of the project show that it is indeed possible to push the particles further away from the center of the channel, however at the expense of raising the shear stress in the system. The best achieved result was a 40 percent increase in the distance from the center line. Provided that a physically fabricated version of the optimized chip works as well as the simulations showed, this would make the acoustophoresis method more clinically viable.**

I. Introduction

CANCER is one of the most common causes of death in Sweden, with an age-standardized mortality rate of 257 deaths per 100 000 men and 198 deaths per 100 000 women in a given year. This is second only to cardiovascular diseases, which cause 328 deaths per 100 000 men and 214 deaths per 100 000 women in a given year, adjusted for age [1]. In addition to the high mortality rate, there is reason to believe that the incidence of cancer is on the rise [2].

A. Circulating tumor cells

Malignant tumors that have yet to metastasize can be removed with surgery or radiotherapy, but once metastatic growth occurs, the spread can destroy vital organs and tissues [3]. Tumor cells that leave the primary tumor and enter into the bloodstream are called Circulating Tumor Cells (CTC) [4]. Previous studies have demonstrated the use of CTCs as a biomarker for different types of metastatic cancer [5]–[9], and model studies have shown that CTCs are present within the bloodstream before other evidence of metastasis is able to be detected [10], [11].

Inlämnat den June 4, 2023
Emejladress:{ch4145pa-s@student.lu.se, jo2876li-s@student.lu.se}
Teknisk handledare: Thierry Baasch, Avdelningen för Biomedicinsk teknik
Swedish title: Optimering av utformning på flödesdelare i mikrofluidiksystem för högre volymflöden

A challenge with detecting CTCs is the low concentration at which they exist in the bloodstream. For a milliliter of blood, there are approximately 1 to 10 CTCs along with billions of red blood cells [4]. The current gold-standard method for detecting CTCs is the CELLSEARCH® method [4], [12], a method that is based on immunomagnetic particles coated in EpCAM antibodies [4], [13]. Epithelial cell adhesion molecules, EpCAM, are membrane proteins found on epithelia [14]. The tumor cells are then identified among the separated epithelial cells through fluorescent staining [4], [13]. However, since not all CTCs express epithelial markers, the technologies that rely upon them may not detect all CTCs present in the sample [15].

B. Acoustophoresis

In order to facilitate the detection of a broader collection of CTC types, acoustophoresis can be used instead of CELLSEARCH® [4]. In a general sense, acoustophoresis is defined as migration by sound [16]. However, in the context of this project, acoustophoresis is more readily defined as a microfluidic technique that uses ultrasonic waves in order to manipulate and separate microparticles or cell populations [4]. It is a label-free method that separates particles based on their physical properties [16] rather than target proteins. This technique can be utilized for manipulation of cell populations [16] and previous works have demonstrated its use in separating tumor cells from red blood cells [17], mononuclear cells from whole blood [18] and red blood cells from lipid particles based on their different compressibility and density [19].

Acoustophoresis can also be used to separate circulating tumor cells (CTCs) from the blood based on their different acoustic mobility, stemming from the difference in radius between CTCs and blood cells [17]. The separation occurs within a microfluidic system placed on a microchip [20], that was produced by deep reactive ion etching in silicon [18]. The microchip this thesis continues to work upon has been described in previous research [18], [20]. The microchip component of interest for this thesis is the inlet fork, pictured in Fig.1. The flow of sample particles enters through the side inlet and flow around the inlet fork (A), a buffer solution flows in through the center inlet (B) and both the flows then exit into the separation channel (C) [20]. At the end of the separation channel there is a “mirrored” outlet fork, here the separated particles exit through the center outlet with the buffer and the remaining sample particles in the side outlet [20].

Intact living cells are important to be able to perform patient CTC lines and functional assays [4]. Therefore, it is important that the separation method has a short processing time in order

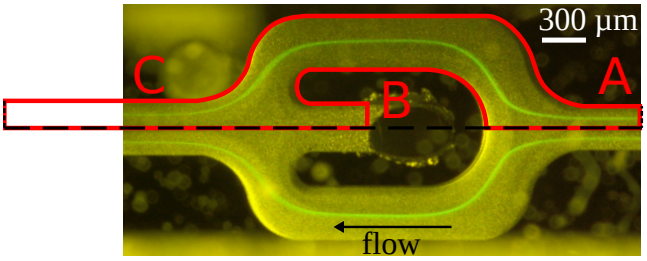

Figure 1. Bright field microscopy image of the inlet fork with the traced sketch overlay (Courtesy of Thierry Baasch) [20].

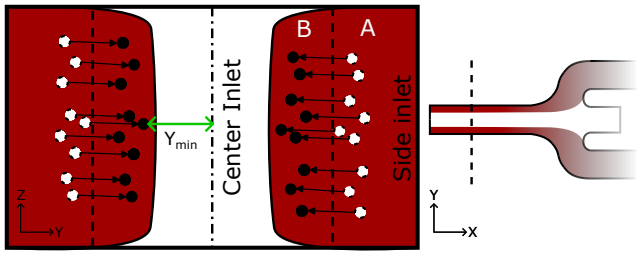

Figure 2. The dashed line in the right overview figure marks the channel cross-section position shown to the left. (A) At low throughput, the boundary between the flows of the side and center inlet is a straight plane. (B) During high throughput, the boundary is deformed and the particles from the side inlet are pushed closer to the center line.

to avoid cell death or alteration [4]. It is also important that the separation method avoids exerting stress on the sample cells, for the same reasons [4]. Hydrodynamic forces can both destroy and induce physiological changes to cells [21]. The normal range of shear stresses CTCs encounter within the circulatory system is between 0.1-0.4 Pa in the venous and 0.4-3 Pa in the arterial circulation [22]. Due to the quick deterioration of the majority of CTCs shed from a tumor into the bloodstream, it has been hypothesized that CTCs are very fragile in terms of shear stress [23]. Previous research have worked to deduce thresholds for initiation of cell lysis, the destruction of cells through the damage or rupture of the cell membrane [24], by shear stress for different cell types. For myeloma cell lines in mice, the threshold for significant lysis was found to be 1800 dyn/cm^2 or 180 Pa (1 Pa = 10 dyn/cm^2) [25]. However, some experiments have shown that CTCs have a remarkably high resistance to momentary exposure to high shear stresses, with little loss in viability for human prostate cancer cells when exposed to approximately 51 Pa [26].

Because of the scarcity of CTCs in whole-blood samples, a sample throughput of 100 $\mu\mathrm{L\,min^{-1}}$ is required to enable isolation of CTC cells in a clinical setting with sample sizes of several milliliters [20]. Microfluidic devices can in principle operate at those increased flow rates, with the prerequisite that the flow remains within the Stokes regime [20]. However, with an increased flow rate, inertial forces begin to have a larger impact on the flow dynamics [20]. Not only does increasing the speed increase the risk of turbulent flow, it also increases the risk of a phenomenon called *the spillover effect*.

The *spillover effect*, illustrated in Fig.2, occurs when the total flow rates exceed a critical level and interferes with the acoustic separation [20]. At low fluid throughput (Stokes flow) the surface that separates the side and center inlet flows is a flat plane. When the fluid throughput is increased, inertial forces begin to deform the separating surface, pushing the side inlet flow closer to the center [20]. Ultimately, the particles can get so close to the center line that they exit through the center outlet without the influence acoustophoresis [20]. This is detrimental as it makes certain flow settings inefficient or impossible to use. Previous studies have concluded that the spillover effect could be reduced by optimizing the channel geometry [20]. One way of optimizing the channel geometry is using genetic algorithms.

C. *Optimization with genetic algorithms*

As the name suggests, the basis of genetic algorithms is to mimic evolution in order to solve optimization problems [27]. The flow graph in Fig.3 details the basic problem-solving strategy for a genetic algorithm. It begins with the creation of an initial population of possible solutions randomly distributed to cover the solution space, the "genetic" material of the solutions can be lists of values or symbols. [27]. The population are then fed through the main loop [27]. In the crossover step, genetic material between solutions are exchanged, the motivation for this being that combining successful parts of two solutions could yield an even better solution [27].

Following the crossover step is the mutation step, which introduces random changes to the genetic material of the solutions [27]. After the mutation step, the fitness step evaluates the performance of each solution through a fitness function provided to the algorithm, the design of which is an integral part of the optimization problem [27]. The computed fitness values are then used in the selection step to create a new "generation" to be used in the next loop iteration [27]. The optimization is terminated when a termination condition is reached, commonly this occurs after a set number of generations or when the improvement in fitness stagnates below a predefined threshold [27].

Genetic algorithms are very useful for problems that cannot be optimized using conventional techniques, such as differentiation [28]. Most real world engineering problems require the use of stochastic optimization techniques because the results that are to be optimized are given as discrete data points. This would make it impossible to solve with conventional optimization techniques, as they require a continuous objective function. As such, the optimization in this project is one that is well suited for using a genetic algorithm [29].

Another key part of the optimization is the finite element method, a numerical method for finding approximate solutions to partial differential equations that are too difficult to solve analytically [30]. COMSOL Multiphysics® (henceforth referred to as only "Comsol" in this thesis) is a software that uses the finite element method in order to create models and simulate different kinds of physical phenomena, such as fluid flows. Models can be built with the help of the software or imported from external sources, such as CAD programs [31]. The simulations can be controlled inside the software

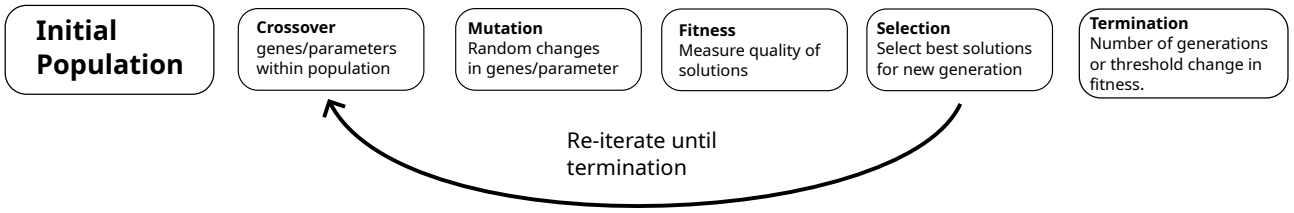

Figure 3. Flow graph of the steps in a simple genetic algorithm.

directly or through MATLAB®, a numeric computing platform [32]. MATLAB® allows for implementing algorithms such as genetic algorithms. A link can be established between the two pieces of software with the help of the LiveLink™ interface, making it possible to use genetic algorithms on Comsol models [33].

Acoustofluidics involves the application of forces to particles with ultrasound within a microfluidic system [34]. A previous thesis implemented an optimization routine for optimal pressure distributions in an acoustofluidic device [29]. Said thesis utilized the LiveLink™ interface to connect a MATLAB® genetic algorithm implementation with COMSOL Multiphysics®, allowing the fitness function to incorporate calculations based on a simulated microfluidic device setup [29]. The achieved solutions were consistent to theory and previously published results [29].

Because of previous successes in optimizing field parameters like pressure with new channel geometries suggested by genetic algorithms. The goal of the underlying work is to decrease the spillover effect by optimizing the channel geometry using genetic algorithms. This would allow for an increased flow throughput, which would in turn enable swift processing of samples, increasing the method's viability for separation of CTC cells.

First, the process of setting up the optimization procedure will be explained. The results of the optimization attempts will be shown and discussed in depth. The final section consists of concluding whether the thesis holds.

II. Method

The numerical setup created for evaluating the model was based upon a procedure presented in previous work within the field [29], generalizing it to support a larger array of models and fitness function implementations. For this thesis, COMSOL Multiphysics® version 6.1 was used, along with several versions of MATLAB®. All the code mentioned in this report works on the versions R2022a, R2022b and R2023b. The link between MATLAB® and COMSOL Multiphysics® was established using the LiveLink™ for MATLAB®.

A base COMSOL model was created based on a sketch of the actual inlet fork seen in Fig.1. The sketch was produced in a previous experiment by overlaying a picture taken of the experimental setup [20]. The transition from sketch to COMSOL model was made using the COMSOL Multiphysics® CAD import functionality, which allows geometry to be imported from AutoCAD® DXF™ (.dxf) files. The sketch which was saved in the Scalable Vector Graphics (.svg) file format

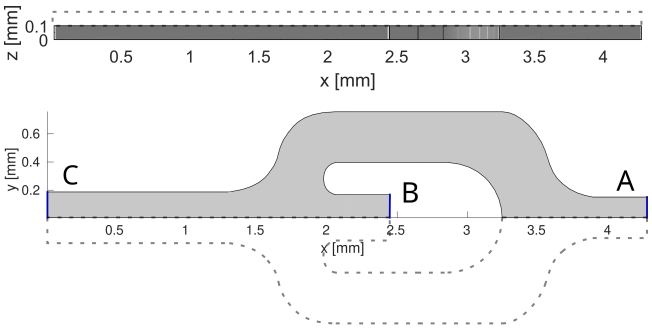

Figure 4. Geometry and physics setup of the base model created in Comsol: (A) Side inlet (B) Center inlet (C) Outlet into separation channel. The two symmetries in the model are marked with dashed lines.

therefore had to be converted into a .dxf file before import, this was achieved with the vector graphics software Inkscape. The final base model geometry is visible in Fig.4.

The physics setup of the model were similar to a previously published model [20]. For the physics simulation, the base model used the laminar flow physics interface in Comsol set to incompressible flow. The density of the fluid was set to 1000 $\mathrm{kg\,m^{-3}}$ and the dynamic viscosity 0.00101 $\mathrm{Pa\,s}$. The total fluid throughput Q_T was set to 2000 $\mu\mathrm{L\,min^{-1}}$ in order to emphasize the spillover effect. The boundary condition for both inlets were set to fully developed flow, with the side inlet (Fig.4A) flow rate set to $Q_{s,in} = 0.25 \times r \times Q_T$ and the center inlet (Fig.4B) flow rate set to $Q_{c,in} = 0.25 \times (1 - r) \times Q_T$, with the splitting ratio r between the two inlets being set to 0.5. For the outlet into the separation channel (Fig.4C) the boundary condition was set to a static pressure of 0 Pa. The boundary condition of the enclosing geometry of the channel were set to no slip. The base model featured two planes of symmetry, one along the xy-plane and one along the xz-plane (Fig.4). Utilizing the symmetry of the fork made it possible to only create a model of a quarter of the fork without losing any information, which decreased the computation time significantly [20]. Therefore, the factor 0.25 for the flow rates were added to account for these symmetries.

Subsequent COMSOL models were based on this base model, replacing fixed segments of the base geometry with parameterized counterparts. To better illustrate this process, consider the example in Fig.5, showing the first parameterization done for the thesis. Beginning with the base model, the 90° curve marked as a dashed line was removed. In place of the dashed curve, a quadratic Bézier curve, corresponding to the curve marked in red, was added. The quadratic Bézier

Figure 5. The base model segment drawn with dashes and the parameterized quadratic Bézier curve in red with the middle control point.

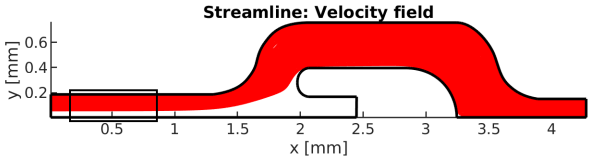

Figure 6. Particle streamline from the side inlet to outlet, simulated in COMSOL Multiphysics®. The black box marks the area of streamline positions used in the fitness function.

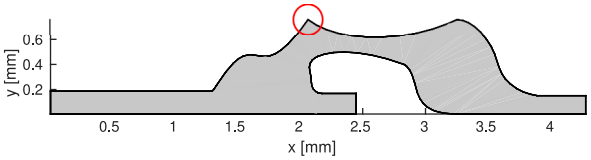

Figure 7. The vertex highlighted in red has a fillet applied with radius 0.795 mm, but in combination with the other applied parameters results in a warning and therefore remains unset, leaving a sharp turn.

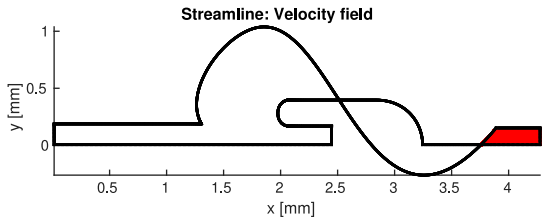

Figure 8. Suggested solution with intersecting geometry segments due to insufficient constraints on parameters. Streamlines fail to progress to outlet.

curve in COMSOL is defined by three control points, the start, and end points were fixated to coincide with the adjacent curves in order to form a closed shape. The two-dimensional coordinates for the middle control point became the parameters for this model, allowing the genetic algorithm to control the position with some spatial constraints, keeping the control point from intersecting through walls.

The fitness function defined for the optimization problem is tied to the spillover effect. Since the spillover effect moves the particles closer to the center of the channel as illustrated in Fig.2, the distance between the center line and the closest particle streamline seen in Fig.6 was defined as Y_{min} (Shown in Fig.2). By convention, a better fitness score has a lower numerical value, therefore y^{-1} was chosen as the fitness score. This means that the further the closest particle is to the center line, the lower the numerical value becomes and better the fitness. In order to avoid the possibility that the minimal y-value occurs somewhere in the inlet of the channel, the scope of the y-value was limited to particles with x coordinates beyond the inlet part of the fork in the separation channel, see the black box in Fig.6.

This fitness function was implemented in $inletForkBulkFit.m$ and was referred to as the "bulk" approach. A slightly modified version for pre-focused particles is explored in Appendix A. The streamline plot seen in Fig. 6 was added to each model through the LiveLink™ API as a new plot group "pgFit" with 100 streamlines originating from the inlet (See Fig.4) surface. The discrete 3D streamline coordinates were later retrieved by extracting the "pgFit" plot data through the $mphplot$ function [33]. The x and y coordinates were fed into the $inletForkNearestY.m$ function that computed the nearest y coordinate to the channel center within the channel section marked in the black box in Fig.6.

In the event that the COMSOL simulation did not finish, the fitness score was set to positive infinity with Inf (MATLAB® scalar representation of positive infinity [35]). This occurred when COMSOL ran into an unrecoverable error. Either when the solution did not converge or if the parameterization suggested by the genetic algorithm resulted in an invalid geometry, such as intersecting geometry segments seen in Fig.8. Each solution had to be assigned a fitness score, therefore the solutions generating errors were assigned a fitness value of Inf effectively discarding them.

Besides errors, some parametrization combinations caused COMSOL warnings. COMSOL warnings differ in their severity compared to errors, and generally did not prevent a model study from being run. However, if a parameter value set to a node generated a warning the parameter would be reset without throwing an error, giving the algorithm a false impression that the parametrization had been successfully applied. An example of this is seen in Fig.7, the fillet value of the corner marked in red is non-zero, but since it causes a warning it is not applied and the corner is left sharp. Since the warnings led to algorithm solutions with mismatch between the parametrization values and the actual model, they were treated the same as errors in terms of fitness, i.e., assigning it to Inf.

Finally, some invalid geometry was neither caught through warnings nor errors, and they were able to progress through the computational step. Fig.8 is such an example, the simulation succeeded, but the streamlines were blocked from flowing towards the outlet by the invalid geometry. These solutions were circumvented by checking the plot data returned from COMSOL Multiphysics® and making sure there were streamline positions in the separation channel (between 0.2 mm and 0.7 mm, see Fig.8).

For a COMSOL model, the number of errors and warnings reported can be checked with the LiveLink™ function $mphshowerrors(model)$ [33]. However, in the case of the models built for this thesis, the provided function proved unable to identify models that contained warnings, even ones that had been verified by the Comsol GUI to cause warnings. This led to the implementation of a new routine for checking for warnings, $inletForkFitWarn.m$, that iterated through each of the geometry nodes, checking them separately with

the $problems$ node property [31].

A MATLAB® program $optimize.m$ was implemented with the ability to perform the optimization on different parameterization setups described by structures inheriting from a "base" model class, utilizing polymorphism to apply the parameterization. The program also included functionality with parallel processing similar to previous works [29] in order to increase the processing speed of the optimization routine. This was accomplished by a combination of the MATLAB® Parallel Computing Toolbox [36] along with starting several COMSOL servers on different ports. Each MATLAB® worker was then connected to a separate COMSOL server. In the interest of saving RAM, the program was written in such a way that the internal memory clears after each generation. This enabled the optimization to run for tens of generations, even if the population sizes were large, without causing a crash. The genetic algorithm was implemented with the MATLAB® Global Optimization Toolbox [36], and was configured using the MATLAB® $optimoptions$ function. $PopulationSize$ and $MaxGenerations$ was set through user input while $UseParallel$ was set to $true$ if parallelism was enabled, rest of the configuration options were left as default.

A further development of this setup in this thesis was to handle disconnecting for the COMSOL server after the optimization problem had ended, which allowed the optimization to be started again without the need for $clearall$ in MATLAB®. Model configuration within MATLAB® were done with subclasses of a Model super class. In these subclasses, the fitness function, number of parameters, boundaries, and optional linear constraints were specified to be provided in the MATLAB® genetic algorithm entry point ga in $optimize.m$. The corresponding COMSOL model path was also provided through the model subclass.

Optimization commenced after the completion of the setup. As mentioned earlier, all the models that were tested were expansions of the base model. 24 models of varying complexity were built and tested. In order to keep track of the models without having to use the names, every saved instance of a model was assigned an ID number. All the models were tested in the same manner, by letting the genetic algorithm run for a population size of five and two generations. The models were evaluated based on the initial fitness values as to determine whether the model had potential. Models that showed no considerable improvement over the base model were discarded so that time and effort could be focused on models with viability.

In order to save time, the result of an optimization was automatically saved to a table in .csv format using a MATLAB® script, $resultSaver.m$. In $resultSaver.m$, the existing result table is imported using the $readTable$ function, resized if necessary, updated with the new result and then saved using the $writeTable$ function. A MATLAB® function was then written to automatically apply the parameters saved from the previous optimization result into a LiveLink™ COMSOL model. This allowed for instant visualization of the result. Apart from the fitness values, the result tables detail every entry's model name, population number, number of generations, time and genetic algorithm configuration parameters. This was done in order to create a good overview of how the models compared to each other, making it easier to predict what parameterization setups would work when it was time to progress to new models.

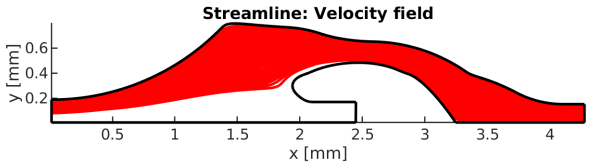

Figure 9. Particle streamlines for the model that achieved the best fitness.

To estimate the magnitude of shear stresses that cells would experience traveling through a channel geometry, Comsol was used to compute an approximate mean and maximum value through LiveLink™. The approximate value was expressed as the multiplication of the dynamic viscosity (*spf.mu* [Pa s)]) and the shear rate (*spf.sr* [s^{-1}]) of the laminar flow physics interface. The shear rate was in turned calculated as

$$spf.sr = \sqrt{2 \times (\sum_{i=1}^{3}\sum_{j=1}^{3} E_{ij}^2) + eps}$$

where E_{ij} is the strain tensor and eps the Comsol floating point accuracy. This expression was evaluated over the entire channel volume with LiveLink™ commands $mphmean$ and $mphmax$ to compute the approximate mean and max values.

The source code in its entirety for the optimization routine and the tools developed for managing and visualizing the results are available in an online git repository [37].

III. Results

A table containing the fitness, population, and generation count and computation time of the 5 highest performing models, along with the base model, are summarized in Table I. The best performing model by fitness was the $HeptaFilletTripleCBezier$ model with a fitness score of 11.2059. This amounts to an increase of 0.0255 mm in distance from the channel center line for the closest streamline compared to the base model, which corresponds to a 40% increase. The streamline plot for the highest performing model is visible in Fig.9. A comparison of the streamline positions seen from the cross-section of the separation channel is plotted in Fig.10, in terms of y coordinate positions along the z axis the optimized model is more evenly distributed compared to the base model.

The maximum and average approximate shear stress in the top 5 performing models along with the base model were calculated and is visible in Table II, for the best performing model the approximate max shear stress was 54.7856 Pa and the average 3.4997 Pa, which was an increase over the base model which had a maximum approximate shear stress of 25.6407 Pa and average of 4.0253 Pa. The approximate shear stress distribution measured in pascals of the best performing model is available in Fig.11.

A variational analysis of the results in Table I were performed and is available in Appendix B.

ID	Model	Parameters	Fitness	Population	Generations	Time (min)
47	HeptaFilletTripleCBezier	25	11.2059	350	20	785.2974
41	HexaFilletTripleCBezier	24	11.5171	144	15	190.086
40	InterpolationOuterInner	12	11.8694	36	15	337.3988
38	InterpolationOuter2	8	11.9163	24	15	224.5714
46	NonaFilletModel	9	13.87	45	10	90.03
4	BaseModel	0	15.6922			

Table I
RESULTS FROM MODEL OPTIMIZATION ORDERED BY FITNESS SCORE.

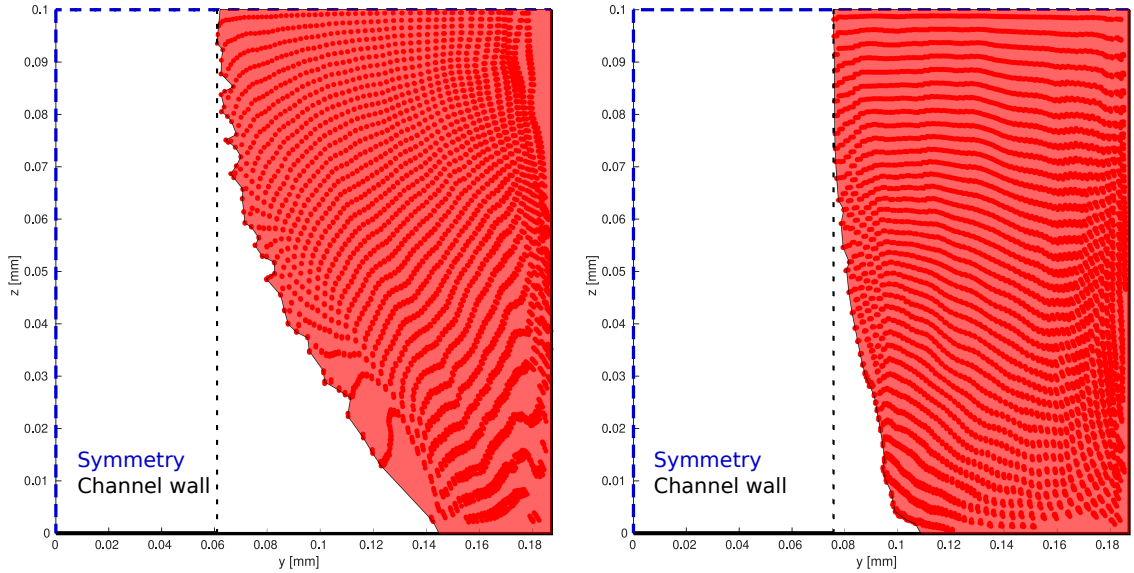

Figure 10. Streamline position distribution of 2000 streamlines in the cross-section of the far left portion of the separation channel. Base model to the left and best performing optimized model to the right.

ID	Max Shear Stress (Pa)	Avg. Shear Stress (Pa)
47	54.7856	3.4997
41	29.4671	2.8091
40	702.3758	8.0031
38	24.5278	5.7956
46	24.3387	3.6287
4	25.6407	4.0253

Table II
MAXIMUM AND AVERAGE APPROXIMATE SHEAR STRESSES FOR THE TOP FIVE PERFORMING MODELS AND THE BASE MODEL.

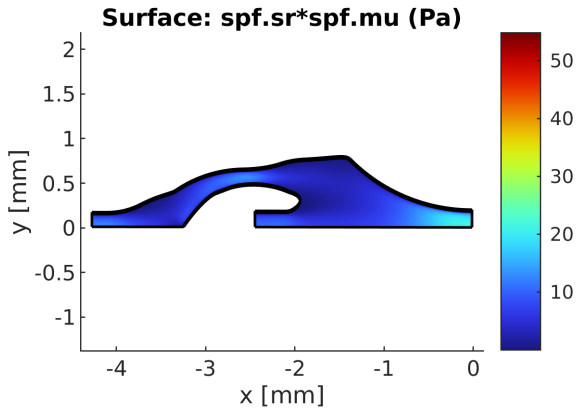

Figure 11. Approximate shear stress distribution of the simulated chip in Pascal.

IV. DISCUSSION

A. Genetic algorithm implementation

As previously noted, intact and living cells are important for further analysis steps post separation, and high magnitude hydrodynamic forces have the ability to kill cells in the sample. Therefore, the increase of maximum shear stress with a change in channel geometry compared to the base model is of interest for the solution's viability, in addition to the fitness score. Some models converged to solutions that were good in terms of the defined fitness function, but that resulted in very high approximate maximum shear stresses, which could be detrimental for cell viability. An extreme example of this is visible in Fig.12, a model with a fitness score of 11.0411 that reached a maximum approximate shear stress of 2853.2638 Pa. A further refinement to the fitness function could be to incorporate the approximate maximum shear stress, to suppress solutions with potentially detrimental shear stresses.

In hindsight, the fitness function could have been constructed in a better way. Although it is still useful as a comparison tool, the non-linear nature of the fitness function

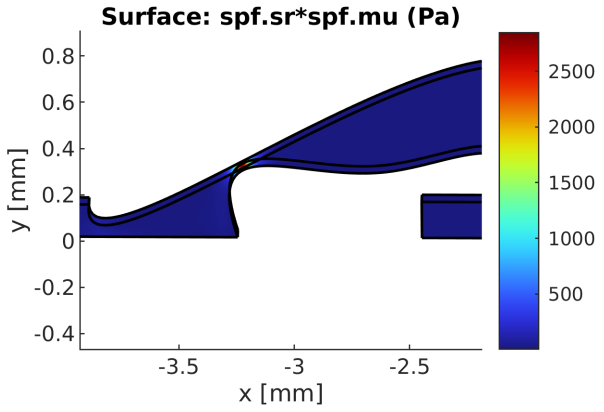

Figure 12. Optimization result with a good fitness score but with very high maximum shear stress.

makes it harder to compare different models than it would have been if a linear fitness function was used instead. In addition to these problems, there is also reason to suspect that it has caused models to be discarded prematurely due to improvements being perceived as smaller than they actually were. If the project was to be redone, maximizing the y value would probably be a better strategy, as this would result in a linear fitness function. Another idea would be minimizing the value between the upper wall and Y_{min}, as this renders a fitness function that is not only linear but also defined all the way to 0.

The default genetic algorithm configuration was used throughout this thesis, a further development could be to explore alternatives in regard to initial population creation, selection, mutation and crossover functions available in the MATLAB® Global Optimization Toolbox [36].

B. Sustainability

As mentioned in the introduction, the chips used in this process are made using silicon. Silicon is abundant in Earth's crust, being the second most common element after oxygen [38]. Although it is abundant, the mining has a concerning environmental impact. Land deterioration, loss of biodiversity and pollution are among the major concerns of the silicon extraction industry [39]. Another concerning factor is the fact that silicon reserves are concentrated in nations such as China and Russia, [40] both of which have had sanctions put on them by the west due to Russia's actions in Ukraine and China's support thereof. These aspects are concerning, but to what extent the numerical results will impact the dependency of silicon will be better understood post fabrication [41].

As an alternative to silicon, several biodegradable and biocompatible materials have been used for the manufacturing of lab on a chip microchips [42]. Applications include laser etched and coated channels in wood for fluorescence detection of proteins [43], cell culturing in devices made from gelatin [44] and Rhodamine B gradient generation with a microchip design fabricated from corn proteins for use in the agricultural sector [45].

C. Ethics

Besides the microfluidic applications described thus far in this thesis, the technology could potentially enable applications with ethical concerns. Sex selection technology (SST) aims to control the biological sex of offspring, the procedure is restricted to use in preventing genetic disorders from progressing [46], [47]. In a few countries, an exception is made for "family balancing", achieving a desired variety in biological sex within the family [47], [48]. Methods of SST include different methods of sperm sorting and pre-implantation genetic diagnosis (PGD) [47]. Besides these established methods, microfluidic systems has been shown to be able to trap and label sperm cells based on their chromosomal content with FISH staining [49]. The same method used in the separation setup described in this thesis, acoustophoresis, has been used to orient non-spherical cells like sperm and red blood cells, the former aiding in separation of sperms based on chromosomal content with flow cytometry for herd management [50], [51].

Proponents of the technique argue that it is part of procreative liberty, and that parents should be able to choose if the outcome is of high importance to whether they would procreate in the first place [52]. Opponents argue that the technique reinforces sexism, that large scale adoption of the technique potentially could skew gender demographics and that the technique is a step further down the slope, and could be used to warrant further genetic control in the future [52], [53].

V. Conclusion

In conclusion, the numerical simulations suggest that it is indeed possible to decrease the spillover effect by changing the shape of the fluid splitter. There is reason to believe that it can be improved even further, at the expense of higher shear stress. Further testing is warranted in order to confirm the validity of the numerical results in a physical copy of the microchip.

VI. Afterword

We would like to thank all the people involved in the course for interesting and useful lectures. A special thanks to Thierry Baasch, our supervisor, and Thomas Laurell for invaluable support and feedback throughout the entire project.

As for division of labor, we have both been involved in all parts of the project. The report writing has been split equally, however, Joel has done most of the programming and Christoffer has done most of the model building in COMSOL.

References

[1] Socialstyrelsen, "Statistics on Causes of Death 2021," 2022. Art.no: 2022-6-8021.

[2] Socialstyrelsen, "Statistik om nyupptäckta cancerfall 2021," 2022. Art.nr: 2022-12-8308.

[3] F. O. Stephens and K. Reinhard Aigner, "What Is Malignancy?," in *Basics of Oncology* (K. R. Aigner and F. O. Stephens, eds.), pp. 3–16, Berlin, Heidelberg: Springer, 2009.

[4] E. Undvall, *Isolation of Circulating Tumor Cells with Acoustophoresis : Towards a biomarker assay for prostate cancer*. thesis/doccomp, Lund University, 2022. ISBN: 9789180391368 9789180391351.

[5] E. Undvall Anand, C. Magnusson, A. Lenshof, Y. Ceder, H. Lilja, and T. Laurell, "Two-Step Acoustophoresis Separation of Live Tumor Cells from Whole Blood," *Analytical Chemistry*, vol. 93, pp. 17076–17085, Dec. 2021. Publisher: American Chemical Society.

[6] D. C. Danila, G. Heller, G. A. Gignac, R. Gonzalez-Espinoza, A. Anand, E. Tanaka, H. Lilja, L. Schwartz, S. Larson, M. Fleisher, and H. I. Scher, "Circulating Tumor Cell Number and Prognosis in Progressive Castration-Resistant Prostate Cancer," *Clinical Cancer Research*, vol. 13, pp. 7053–7058, Dec. 2007.

[7] M. Cristofanilli, G. T. Budd, M. J. Ellis, A. Stopeck, J. Matera, M. C. Miller, J. M. Reuben, G. V. Doyle, W. J. Allard, L. W. Terstappen, and D. F. Hayes, "Circulating Tumor Cells, Disease Progression, and Survival in Metastatic Breast Cancer," *New England Journal of Medicine*, vol. 351, pp. 781–791, Aug. 2004. Publisher: Massachusetts Medical Society _eprint: https://doi.org/10.1056/NEJMoa040766.

[8] H. I. Scher, M. J. Morris, S. Larson, and G. Heller, "Validation and clinical utility of prostate cancer biomarkers," *Nature Reviews Clinical Oncology*, vol. 10, pp. 225–234, Apr. 2013. Number: 4 Publisher: Nature Publishing Group.

[9] S. J. Cohen, C. J. Punt, N. Iannotti, B. H. Saidman, K. D. Sabbath, N. Y. Gabrail, J. Picus, M. Morse, E. Mitchell, M. C. Miller, G. V. Doyle, H. Tissing, L. W. Terstappen, and N. J. Meropol, "Relationship of Circulating Tumor Cells to Tumor Response, Progression-Free Survival, and Overall Survival in Patients With Metastatic Colorectal Cancer," *Journal of Clinical Oncology*, vol. 26, pp. 3213–3221, July 2008. Publisher: Wolters Kluwer.

[10] W. He, H. Wang, L. C. Hartmann, J.-X. Cheng, and P. S. Low, "In vivo quantitation of rare circulating tumor cells by multiphoton intravital flow cytometry," *Proceedings of the National Academy of Sciences*, vol. 104, pp. 11760–11765, July 2007. Publisher: Proceedings of the National Academy of Sciences.

[11] K. Pantel and M. R. Speicher, "The biology of circulating tumor cells," *Oncogene*, vol. 35, pp. 1216–1224, Mar. 2016. Number: 10 Publisher: Nature Publishing Group.

[12] "CELLSEARCH® | Home."

[13] K. Pantel, R. H. Brakenhoff, and B. Brandt, "Detection, clinical relevance and specific biological properties of disseminating tumour cells," *Nature Reviews Cancer*, vol. 8, pp. 329–340, May 2008. Number: 5 Publisher: Nature Publishing Group.

[14] M. A. Chaudry, "EpCAM," in *Encyclopedia of Cancer* (M. Schwab, ed.), pp. 1540–1549, Berlin, Heidelberg: Springer, 2017.

[15] A. D. Rhim, E. T. Mirek, N. M. Aiello, A. Maitra, J. M. Bailey, F. McAllister, M. Reichert, G. L. Beatty, A. K. Rustgi, R. H. Vonderheide, S. D. Leach, and B. Z. Stanger, "EMT and Dissemination Precede Pancreatic Tumor Formation," *Cell*, vol. 148, pp. 349–361, Jan. 2012.

[16] A. Lenshof and T. Laurell, "Acoustophoresis," in *Encyclopedia of Nanotechnology* (B. Bhushan, ed.), pp. 45–50, Dordrecht: Springer Netherlands, 2012.

[17] C. Magnusson, P. Augustsson, A. Lenshof, Y. Ceder, T. Laurell, and H. Lilja, "Clinical-Scale Cell-Surface-Marker Independent Acoustic Microfluidic Enrichment of Tumor Cells from Blood," *Analytical Chemistry*, vol. 89, pp. 11954–11961, Nov. 2017. Publisher: American Chemical Society.

[18] A. Urbansky, P. Ohlsson, A. Lenshof, F. Garofalo, S. Scheding, and T. Laurell, "Rapid and effective enrichment of mononuclear cells from blood using acoustophoresis," *Scientific Reports*, vol. 7, p. 17161, Dec. 2017. Number: 1 Publisher: Nature Publishing Group.

[19] F. Petersson, A. Nilsson, C. Holm, H. Jönsson, and T. Laurell, "Separation of lipids from blood utilizing ultrasonic standing waves in microfluidic channels," *Analyst*, vol. 129, pp. 938–943, Sept. 2004. Publisher: The Royal Society of Chemistry.

[20] E. Undvall, F. Garofalo, G. Procopio, W. Qiu, A. Lenshof, T. Laurell, and T. Baasch, "Inertia-Induced Breakdown of Acoustic Sorting Efficiency at High Flow Rates," *Physical Review Applied*, vol. 17, p. 034014, Mar. 2022. Publisher: American Physical Society.

[21] Y. Chisti, "Hydrodynamic Damage to Animal Cells," *Critical Reviews in Biotechnology*, vol. 21, pp. 67–110, Jan. 2001. Publisher: Taylor & Francis _eprint: https://doi.org/10.1080/20013891081692.

[22] D. Wirtz, K. Konstantopoulos, and P. C. Searson, "The physics of cancer: the role of physical interactions and mechanical forces in metastasis," *Nature Reviews. Cancer*, vol. 11, pp. 512–522, June 2011.

[23] B. L. Krog and M. D. Henry, "Biomechanics of the Circulating Tumor Cell Microenvironment," in *Biomechanics in Oncology* (C. Dong, N. Zahir, and K. Konstantopoulos, eds.), Advances in Experimental Medicine and Biology, pp. 209–233, Cham: Springer International Publishing, 2018.

[24] "lysis." ISBN: 9780191727016.

[25] A. McQueen, E. Meilhoc, and J. E. Bailey, "Flow effects on the viability and lysis of suspended mammalian cells," *Biotechnology Letters*, vol. 9, pp. 831–836, Dec. 1987.

[26] J. M. Barnes, J. T. Nauseef, and M. D. Henry, "Resistance to Fluid Shear Stress Is a Conserved Biophysical Property of Malignant Cells," *PLOS ONE*, vol. 7, p. e50973, Dec. 2012. Publisher: Public Library of Science.

[27] O. Kramer, "Genetic Algorithms," in *Genetic Algorithm Essentials* (O. Kramer, ed.), Studies in Computational Intelligence, pp. 11–19, Cham: Springer International Publishing, 2017.

[28] MathWorks®, "Genetic Algorithm."

[29] O. Schwab, *Optimization of Ultrasonic Particle Manipulation Devices*. Semester Thesis, Swiss Federal Institute of Technology Zurich, May 2013.

[30] G. R. Liu and S. S. Quek, "Chapter 1 - Computational Modeling," in *The Finite Element Method (Second Edition)* (G. R. Liu and S. S. Quek, eds.), pp. 1–11, Oxford: Butterworth-Heinemann, Jan. 2014.

[31] COMSOL, "COMSOL Multiphysics Programming Reference Manual." Comsol version 6.1.

[32] "MATLAB - MathWorks."

[33] COMSOL, "LiveLink for MATLAB User's Guide." Comsol version 6.1.

[34] H. Bruus, "Governing Equations in Microfluidics," in *Microscale Acoustofluidics* (T. Laurell and A. Lenshof, eds.), p. 0, The Royal Society of Chemistry, Dec. 2014.

[35] "Create array of all Inf values - MATLAB Inf - MathWorks Nordic."

[36] "Global Optimization Toolbox Documentation - MathWorks Nordic."

[37] "jollescott/fluid-splitter-optimization: Bachelor's thesis project: Microfluidic flow splitter shape optimization for high throughput."

[38] Britannica Academic, "silicon (Si)."

[39] A. Mishra, "Impact of silica mining on environment," *Journal of Geography and Regional Planning*, vol. 8, pp. 150–156, June 2015. Publisher: Academic Journals.

[40] "Mineral commodity summaries 2023," tech. rep., 2023.

[41] U.S. Department of the Treasury, "Treasury Imposes Swift and Severe Costs on Russia for Putin's Purported Annexation of Regions of Ukraine," Sept. 2022.

[42] M. Rothbauer, E. I. Reihs, A. Fischer, R. Windhager, F. Jenner, and S. Toegel, "A Progress Report and Roadmap for Microphysiological Systems and Organ-On-A-Chip Technologies to Be More Predictive Models in Human (Knee) Osteoarthritis," *Frontiers in Bioengineering and Biotechnology*, vol. 10, June 2022. Publisher: Frontiers Media S.A.

[43] A. Andar, M.-S. Hasan, V. Srinivasan, M. Al-Adhami, E. Gutierrez, D. Burgenson, X. Ge, L. Tolosa, Y. Kostov, and G. Rao, "Wood Microfluidics," *Analytical Chemistry*, vol. 91, pp. 11004–11012, Sept. 2019. Publisher: American Chemical Society.

[44] A. Paguirigan and D. J. Beebe, "Gelatin based microfluidic devices for cell culture," *Lab on a Chip*, vol. 6, pp. 407–413, Feb. 2006. Publisher: The Royal Society of Chemistry.

[45] J. Luecha, A. Hsiao, S. Brodsky, G. L. Liu, and J. L. Kokini, "Green microfluidic devices made of corn proteins," *Lab on a Chip*, vol. 11, pp. 3419–3425, Oct. 2011. Publisher: The Royal Society of Chemistry.

[46] World Health Organization, "Preventing gender-biased sex selection: an interagency statement - OHCHR, UNFPA, UNICEF, UN Women and WHO," tech. rep., World Health Organization, 2011. ISBN: 9789241501460 number-of-pages: vi, 19.

[47] O. Kudina, "Accounting for the Moral Significance of Technology: Revisiting the Case of Non-Medical Sex Selection," *Journal of Bioethical Inquiry*, vol. 16, pp. 75–85, Mar. 2019.

[48] M. Bayefsky and B. Jennings, *Regulating Preimplantation Genetic Diagnosis in the United States: The Limits of Unlimited Selection*. Springer, Jan. 2015. Google-Books-ID: gTlEBgAAQBAJ.

[49] B. d. Wagenaar, J. T. W. Berendsen, J. G. Bomer, W. Olthuis, A. v. d. Berg, and L. I. Segerink, "Microfluidic single sperm entrapment and analysis," *Lab on a Chip*, vol. 15, pp. 1294–1301, Feb. 2015. Publisher: The Royal Society of Chemistry.

[50] O. Jakobsson, M. Antfolk, and T. Laurell, "Continuous Flow Two-Dimensional Acoustic Orientation of Nonspherical Cells," *Analytical Chemistry*, vol. 86, pp. 6111–6114, June 2014. Publisher: American Chemical Society.

[51] J. C. Sharpe and K. M. Evans, "Advances in flow cytometry for sperm sexing," *Theriogenology*, vol. 71, pp. 4–10, Jan. 2009.

[52] J. A. Robertson, "Preconception Gender Selection Target Article," *American Journal of Bioethics*, vol. 1, no. 1, pp. 2–9, 2001.

[53] C. Strong, "Can't You Control Your Children? Open Peer Commentaries," *American Journal of Bioethics*, vol. 1, no. 1, pp. 12–13, 2001.

APPENDIX A
PRE-FOCUSED PARTICLES

The approach for pre-focused particles was based on the "bulk" approach, but with only a single particle streamline emanating from the side inlet. Fig.13 details the streamline start position, seen from the channel cross-section at the side inlet (See Fig.4A). The streamline was positioned in the center of the inlet along the y-axis, and slightly below the model channel height along the z-axis, in order for it to be in the center when accounting for the model symmetries. With the "focused" approach, the base model achieved a fitness of 10.1964 while the best performing "bulk" model *HeptaFilletTripleCBezier* seen in Fig.14 achieved a fitness score of 6.9482. This amounted to an increase of distance to the centerline of 0.0458 mm, which corresponds to an 46.7% improvement. These fitness scores are not comparable with the "bulk" scores, since the fitness function has been redefined.

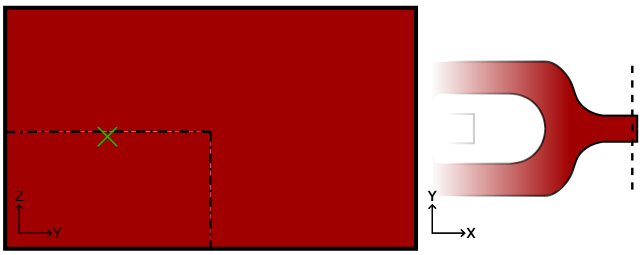

Figure 13. Focused particle streamline position within inlet fork. The dashed line within the cross-section marks the "fourth" of the channel that is being simulated (See the symmetries in Fig.4). The green X marks the origin position of the streamline.

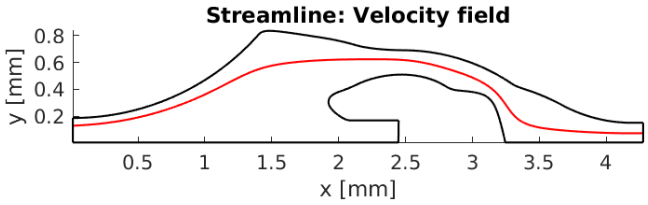

Figure 14. Focused particle streamline for *HeptaFilletTripleCBezier* model.

APPENDIX B
VARIATIONAL ANALYSIS

A testing function, $varAnalysis.m$, was developed in order to determine how stable the results were. It then goes through every parameter of a chosen model, one by one, and tests the impact of changing the parameter. The impact is tested by running two studies, one corresponding to increasing the parameter value with five percent and one corresponding to decreasing the parameter value with five percent. Each study renders a fitness result which is compared with the fitness of the initial model in order to give a value on the perceptual change. The fitness results of these studies are averaged and saved in an array.

In order to facilitate the comparison between different models, a mean value and a max value is also saved in the array. Apart from being a way to measure how stable the results were, the script also made it possible to compare the different parameters of a model. The parameters with higher values are the ones that are most sensitive to change, which is valuable information if one needs to change the model constraints.

Each of the results in Table I were run through a stability analysis and the results are available in Table III. The values are reported as the deviation in percent from the result fitness score when slightly varying the parameters individually. Some variations caused warnings or errors in Comsol, which resulted in a fitness change of *inf*.

ID	47	41	40	38	46
P1	0.66	inf	19.49	27.98	0.63
P2	0.65	-0.49	17.86	32.13	0.62
P3	inf	inf	inf	33.00	0.51
P4	inf	inf	21.61	33.19	inf
P5	inf	inf	inf	29.80	0.60
P6	inf	inf	inf	32.39	0.59
P7	inf	-0.43	22.48	32.66	0.51
P8	0.31	-0.89	20.11	31.95	0.59
P9	1.05	-0.23	inf		0.38
P10	0.92	-0.31	21.20		
P11	0.86	inf	inf		
P12	0.53	inf	inf		
P13	0.74	-0.60			
P14	0.32	-0.64			
P15	0.50	-0.57			
P16	0.40	-0.42			
P17	inf	-0.57			
P18	0.75	-0.42			
P19	0.64	-0.53			
P20	0.65	-0.73			
P21	0.35	-0.56			
P22	0.60	-0.42			
P23	inf	inf			
P24	0.99	-0.54			
P25	0.61				

Table III
FITNESS CHANGE IN PERCENTS WHEN VARYING EACH PARAMETER (P1-25) INDIVIDUALLY. A VALUE OF *inf* MEANS THAT THE PARAMETER CHANGE CAUSED A WARNING OR ERROR IN THE COMSOL MODEL.